Magnetic Field and Cogging Torque Analysis of Surface Permanent Magnet Synchronous Machine using Analytical Method

Hoon-Ki Lee[1], Jong-Hyeon Woo[1], Hyo-Seab Shin[1], Kyung-Hun Shin[2], and Jang-Young Choi[1]*

[1]Chungnam National University, 99 Daehak-ro, Yuseong-gu, Daejeon 34134, Republic of Korea
[2]Chonnam National University, 50, Daehak-ro, Yeosu-si, Jeollanam-do 59626, Republic of Korea

This paper presents the magnetic flux density and cogging torque calculation of a surface permanent magnet synchronous machines. We obtained analytical magnetic field solutions produced by permanent magnets based on the magnetic vector potential. Then, the analytical solutions for cogging torque were obtained. All analytical results were validated with two-dimensional finite element analysis and experimental results.

Keywords : analytical method, magnetic flux density, cogging torque

1. Introduction

Permanent magnet synchronous machines (PMSMs) have become an essential technology in industries such as home appliances, computer peripherals, industrial tools, and electrical vehicles [1-5]. Research on the design and characteristics of PMSMs is being actively conducted. Typically, finite element methods and analytical methods are employed for designing a permanent magnet synchronous motor or performing characteristic analysis. The finite element method is one of the numerical methods that can be performed using a commercial tool, which simplifies the analysis. However, it is necessary to learn how to use each of the required commercial tools. It poses a disadvantage because it becomes difficult and depends on the experience of the designer [6-9]. The analytical method is implemented to analyze the electromagnetic field characteristics using Maxwell's equation. Magnetization modeling using the Fourier series and partial differential equation derived through the magnetic vector potential are applied to the shape of the device. It has to be preceded by deriving a solution considering various boundary conditions that fit, but there is a drawback that magnetic saturation cannot be considered. Because the analytical method can predict the characteristic variation according to design parameters, continuous

research is being conducted. Many two-dimensional analysis models for slotless type were proposed in the early research of the analytical method, most of which focused on open circuit analysis [11]. Assuming that the relative permeability of iron is infinite, slotless permanent magnet machines are very simple; therefore, the magnetic field in the air-gap can be predicted by calculating the Poisson's and Laplace's equations in a simple domain. One of the difficulties in analyzing permanent magnet machines using the analytic method is to consider the slotting effect on the stator side. Energy conversion occurs through a magnetic field in the air gap between the rotor and stator in permanent magnet machines. It is essential to accurately predict magnetic field in the air gap. Slots distort the air gap magnetic field distribution, and the distorted magnetic field distribution has a significant influence on the electromagnetic performance. Therefore, if the permanent magnet machine is analyzed without considering the slotting effect, it is difficult to predict an accurate result of the electromagnetic performance [10-14].

In this study, the governing equation for each domain was derived through the subdomain method, and the magnetic field characteristics in each domain were analyzed. The analysis results were compared with the finite element analysis results to verify the validity of the proposed analysis method.

*Corresponding author: Tel: +82-41-821-7601
Fax: +82-41-821-7601, e-mail: choi_jy@cnu.ac.kr

2. Derivation of Magnetic Field Characteristics and Cogging Torque Characteristics using an Analytical Method

2.1. Analysis model and assumptions

Fig. 1 shows the simplified analysis model and the definition of each region. r_1, r_2, r_3, r_4 and r_5 represent the rotor yoke, surface of permanent magnets, radius of stator, radius of slot-opening, and radius of slot, respectively. β and δ denote a slot-opening angle and an angle occupied by a slot, respectively. θ_i is the ith slot position, which can be expressed by (1) [10]

$$\theta_i = -\frac{\beta}{2} + \frac{2\pi i}{Q} \text{ with } 1 \le i \le Q \tag{1}$$

To apply the analytical method, a process of simplifying the analysis model is required, and the following assumptions are required.
- End effect is neglected.
- Relative permeability of Cores is infinite.
- Relative permeability of a permanent magnet is 1.
- The stator slot has a radial slot

In addition, the analysis model is divided into four regions: a permanent magnet region (Region I), air-gap region (Region II), an ith slot opening region (Region i), and a jth slot region (Region j). According to the afore-mentioned assumptions, the four regions have a structure that is symmetric about the z-direction and are represented in the r-θ coordinate system.

2.2. Magnetic vector potential

Magnetic flux density B, magnetic flux intensity H, and magnetization M exhibit the following relationship [11].

$$\mathbf{B} = \mu_0 \left(\mathbf{H} + \mathbf{M} \right) \tag{2}$$

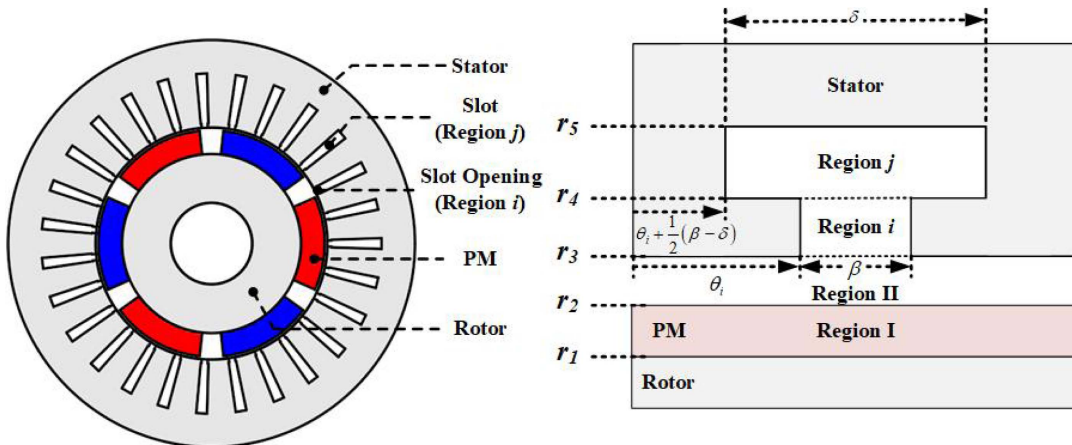By taking curl on both sides of (2), we can obtain (3) as follows.

$$\nabla \times \mathbf{B} = \mu_0 (\nabla \times \mathbf{H}) + \mu_0 (\nabla \times \mathbf{M}) \tag{3}$$

There is no current source in the permanent magnet region. Therefore, is established, which can be summarized as (4).

$$\nabla \times \mathbf{B} = \mu_0 (\nabla \times \mathbf{M}) \tag{4}$$

According to the definition of the magnetic vector potential in (5), (4) can be further summarized as (6), and the left side of (6) is expressed as (7) in a cylindrical coordinate system.

$$\mathbf{B} = \nabla \times \mathbf{A} \tag{5}$$

$$\nabla^2 \mathbf{A} = -\mu_0 (\nabla \times \mathbf{M}) \tag{6}$$

$$\nabla^2 \mathbf{A} = \frac{\partial^2}{\partial r^2}\mathbf{A} + \frac{1}{r}\frac{\partial}{\partial r}\mathbf{A} + \frac{1}{r^2}\frac{\partial^2}{\partial \theta^2}\mathbf{A} + \frac{\partial^2}{\partial z^2}\mathbf{A} \tag{7}$$

2.3. Magnetization modeling
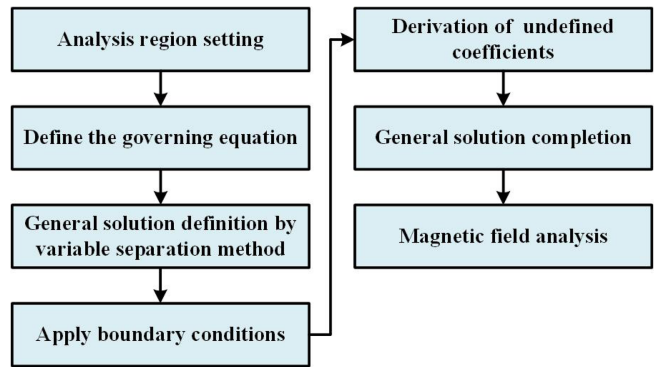
Fig. 3 depicts the Fourier series expansion model for

Fig. 2. (Color online) Analysis flow chart for analytical method.

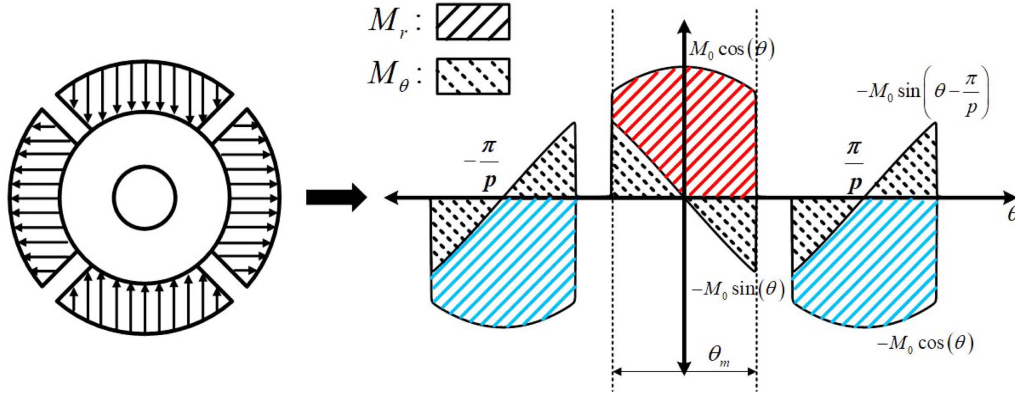**Fig. 1.** (Color online) Simplified analysis model.

Fig. 3. (Color online) Magnetization modeling [15].

the magnetization modeling of a permanent magnet. The Fourier series expansion equation of parallel magnetization is expressed as [2].

$$\mathbf{M} = \sum_{n=1}^{\infty}\left\{ M_{rn}\cos(n(\theta-\theta_0))\mathbf{i}_r + M_{\theta n}\sin(n(\theta-\theta_0))\mathbf{i}_\theta \right\} \quad (8)$$

where n and θ_0 represent harmonic orders and initial position of permanent magnet, respectively. M_{rn} and $M_{\theta n}$ denote the radial and circumferential component of the magnet magnetization, respectively, which can be derived by performing Fourier series modeling, as presented in Fig. 3.

2.4. Derivation of governing equations and general solution

According to the definition of the magnetic vector potential, the governing equation of each domain can be summarized into Poisson's equation and Laplace's equation. Because the magnetization component exists, the magnet region (Region I) can be expressed by the Poisson's equation, and the air-gap region (Region II), slot opening region (Region i), and slot region (Region j) are summarized by the Laplace's equation. The governing equation for each domain is as follows:

$$\frac{\partial^2 \mathbf{A}_{zn}^I}{\partial r^2} + \frac{1}{r}\frac{\partial \mathbf{A}_{zn}^I}{\partial r} + \frac{1}{r^2}\frac{\partial^2 \mathbf{A}_{zn}^I}{\partial \theta^2} = \frac{\mu_0}{r}\frac{\partial \mathbf{M}}{\partial \theta} \quad (9a)$$

$$\frac{\partial^2 \mathbf{A}_{zn}^{II}}{\partial r^2} + \frac{1}{r}\frac{\partial \mathbf{A}_{zn}^{II}}{\partial r} + \frac{1}{r^2}\frac{\partial^2 \mathbf{A}_{zn}^{II}}{\partial \theta^2} = 0 \quad (9b)$$

$$\frac{\partial^2 \mathbf{A}_{zk}^i}{\partial r^2} + \frac{1}{r}\frac{\partial \mathbf{A}_{zk}^i}{\partial r} + \frac{1}{r^2}\frac{\partial^2 \mathbf{A}_{zk}^i}{\partial \theta^2} = 0 \quad (9c)$$

$$\frac{\partial^2 \mathbf{A}_{zm}^j}{\partial r^2} + \frac{1}{r}\frac{\partial \mathbf{A}_{zm}^j}{\partial r} + \frac{1}{r^2}\frac{\partial^2 \mathbf{A}_{zm}^j}{\partial \theta^2} = 0 \quad (9d)$$

The general solutions of the four defined governing equations can be derived using the variable separation method. The general solution is expressed as the product of the function for the radial direction and function for the tangent direction and can be expressed as (10) [6].

$$A(r,\theta) = R(r)\cdot\Theta(\theta) \quad (10)$$

Substituting (10) into (9), the governing equation can be expressed as

$$r^2\frac{R''}{R} + r\frac{R'}{R} = -\frac{\Theta''}{\Theta} = \lambda \quad (11)$$

Where l denotes the variable separation constant. The general solution is as follows:

$$A(r,\theta) = R_0(r)\cdot\Theta_0(\theta) + \sum_{n,k,m=1}^{\infty} R_{n,k,m}(r)\Theta_{n,k,m}(\theta) \quad (12)$$

Therefore, the general solutions for each region can be expressed as

$$\mathbf{A}_{zn}^I = A_0^I + B_0^I \ln r$$
$$+ \sum_{n=1}^{\infty}\left[\begin{array}{l}\left(A_n^I r^{-n} + B_n^I r^n + \frac{\mu_0}{2}r\ln r M_n \cos n\theta_0 \right)\sin(n\theta) \\ + \left(C_n^I r^{-n} + D_n^I r^n - \frac{\mu_0}{2}r\ln r M_n \sin n\theta_0 \right)\cos(n\theta) \end{array} \right] (n=1)$$
$$(13a)$$

$$\mathbf{A}_{zn}^I = A_0^I + B_0^I \ln r$$
$$+ \sum_{n=1}^{\infty}\left[\begin{array}{l}\left(A_n^I r^{-n} + B_n^I r^n + \frac{r\mu_0 n}{(n^2-1)} M_n \cos n\theta_0 \right)\sin(n\theta) \\ + \left(C_n^I r^{-n} + D_n^I r^n - \frac{r\mu_0 n}{(n^2-1)} M_n \sin n\theta_0 \right)\cos(n\theta) \end{array} \right] (n\neq 1)$$
$$(13b)$$

$$\mathbf{A}_n^{II} = A_0^{II} + B_0^{II} \ln r$$
$$+ \sum_{n=1}^{\infty}\left[(A_n^{II} r^{-n} + B_n^{II} r^n)\sin(n\theta) + (C_n^{II} r^{-n} + D_n^{II} r^n)\cos(n\theta) \right]$$
$$(13c)$$

$$\mathbf{A}_k^{so} = A_0^i + B_0^i \ln r + \sum_{k=1}^{\infty} \left[\left(A_k^i r^{\frac{k\pi}{\beta}} + B_k^i r^{\frac{k\pi}{\beta}} \right) \cos\left(\frac{k\pi}{\beta}(\theta - \theta_i) \right) \right]$$

(13d)

$$\mathbf{A}_m^j = A_0^j + B_0^j \ln r$$
$$+ \sum_{m=1}^{\infty} \left[\left(A_m^j r^{-\frac{m\pi}{\delta}} + B_m^j r^{\frac{m\pi}{\delta}} \right) \cos\left(\frac{m\pi}{\delta}\left(\theta - \theta_i - \frac{1}{2}(\beta - \delta) \right) \right) \right]$$

(13e)

where *n*, *k*, and *m* represent the harmonic order of each region.

2.5. Magnetic flux density calculation

Table 1 lists the boundary conditions in analysis regions. When $r = r_1$, the magnetic flux density in the tangential direction is 0 by the Neumann boundary condition, and when $r = r_2$, the continuous boundary condition is applied to equalize the magnetic flux density in the Region I and Region II. When $r = r_3$, the continuous boundary condition and Neumann boundary condition are applied, and the tangential and normal magnetic flux densities of Region *i* and Region II are the same in the slot opening. In addition, in a region other than the slot opening, the magnetic flux density in the tangential direction of the Region I becomes zero. When $r = r_4$, the continuous boundary condition is applied to the slot opening portion, and the Neumann boundary condition is applied to the region other than the slot opening. When $r = r_5$, Neumann boundary condition is applied and the magnetic flux density in the tangential direction becomes 0. Accordingly, the undefined coefficient of the general solution can be derived for each domain, and the magnetic flux density

can be derived by the definition of (5).

2.6. Cogging torque calculation

The force induced in the tangential direction on the stator surface is expressed by the following equation using Maxwell stress tensor [9].

$$\mathbf{F} = \left(\mathbf{i}_n \frac{\mathbf{B}}{\mu_0} \right) \mathbf{B} - \mathbf{i}_n \frac{1}{2} \frac{|\mathbf{B}|^2}{\mu_0}$$

(14)

where **n** and **B** denote the normal direction vector on the stator surface and magnetic flux density on the stator surface, respectively. If (14) is summarized, it can be expressed as follows:

$$\mathbf{F} = \frac{1}{\mu_0} \left(B_r^2 - \frac{1}{2}|\mathbf{B}|^2 \right) \mathbf{i}_r - \frac{1}{\mu_0} B_r B_\theta \mathbf{i}_\theta$$
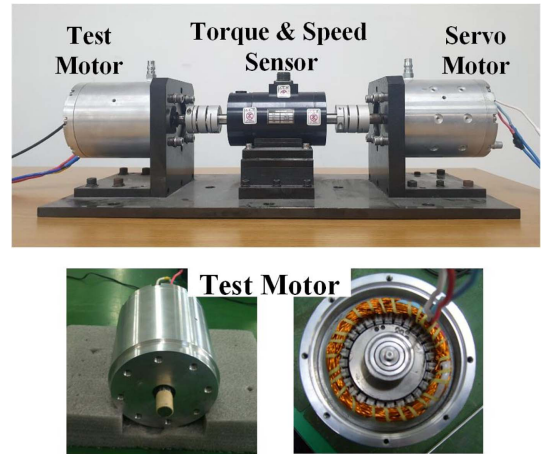
(15)

The normal direction in (15) is used to calculate the radial force, and the tangential direction is used to calculate the torque. Therefore, the torque is derived by

$$T = r F_\theta = \frac{r}{\mu_0} \int_0^{L_{stk}} \int_0^{2\pi} B_r B_\theta r \, d\theta \, dz$$

(16)

where *r* denotes the observation point. B_r and B_q represent normal and tangential component of magnetic flux density at *r*, respectively.

## 3. Comparison and Verification of Analysis Results

Fig. 4 shows the experimental setup and manufacturing model, and Table 2 lists the design specifications. To measure the no-load characteristics, a back to back system was constructed, wherein one servo motor and one test motor were arranged back to back. It is configured to

Table 1. Boundary condition.

$r = r_1$	$B_\theta^I = 0$	-
$r = r_2$	$B_\theta^I = B_\theta^{II}$	-
	$B_r^I = B_r^{II}$	-
$r = r_3$	$B_r^{II} = B_r^i$	$\theta_i < \theta < \theta_i + \beta$
	$B_\theta^i = B_\theta^{II}$	$\theta_i < \theta < \theta_i + \beta$
	$B_\theta^i = 0$	otherwise
$r = r_4$	$B_\theta^i = B_\theta^j$	$\theta_j < \theta < \theta_j + \beta$
	$B_r^i = B_r^j$	$\theta_j < \theta < \theta_j + \beta$
	$B_\theta^j = 0$	otherwise
$r = r_5$	$B_\theta^j = 0$	$\theta_j < \theta < \theta_j + \beta$
$\theta = \theta_i, \theta = \theta_i + \beta$	$B_r^i = 0$	$r_3 < r < r_4$
$\theta = \theta_j, \theta = \theta_j + \delta$	$B_r^j = 0$	$r_4 < r < r_5$

Fig. 4. (Color online) Experimental setup and manufactured model.

Table 2. Design Specification.

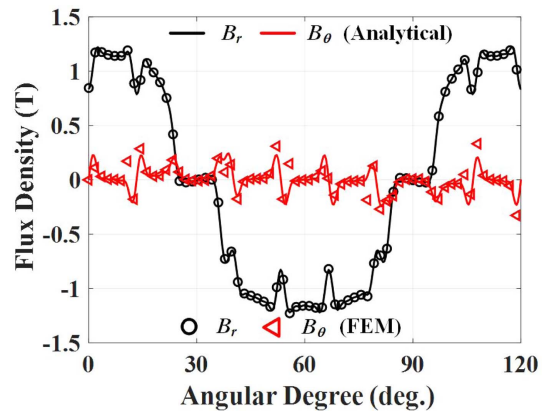| Symbol	Value	Unit
r_1	22	mm
r_2	27.8	mm
r_3	28.5	mm
r_4	29.5	mm
r_5	41.8	mm
L_{stk}	50	mm
β	3	Deg.
δ	3.63	Deg.
B_r	1.28	T
μ_0	$4\pi \times 10^{-7}$	H/m
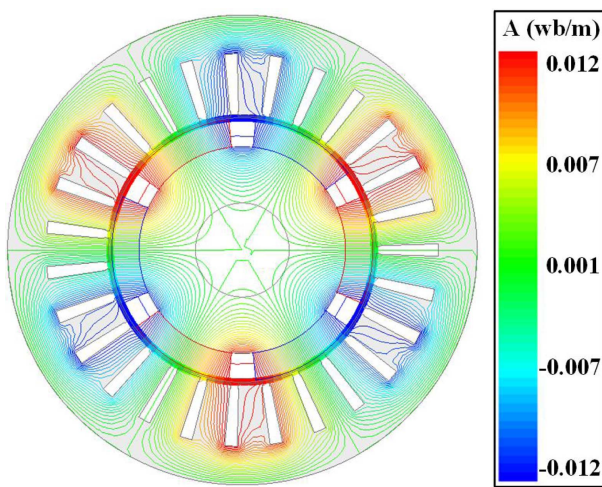
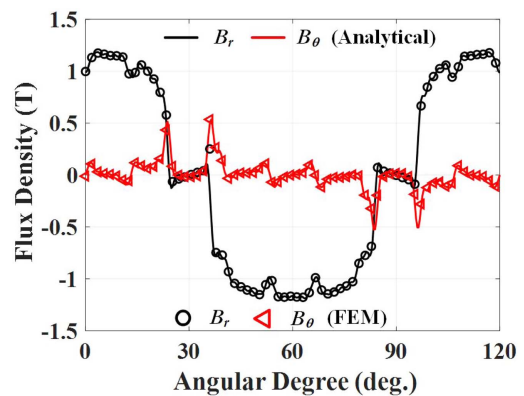**Fig. 5.** (Color online) Magnetic flux line.
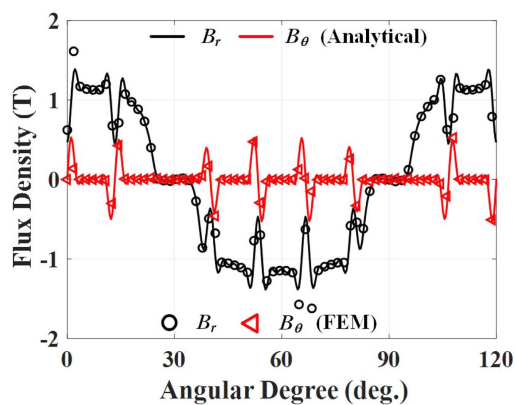
Fig. 6. (Color online) Magnetic flux density distribution at $r = r_3$.

Fig. 7. (Color online) Magnetic flux density distribution at $r = (r_2 + r_3)/2$.

Fig. 8. (Color online) Magnetic flux density distribution at $r = r_2$.
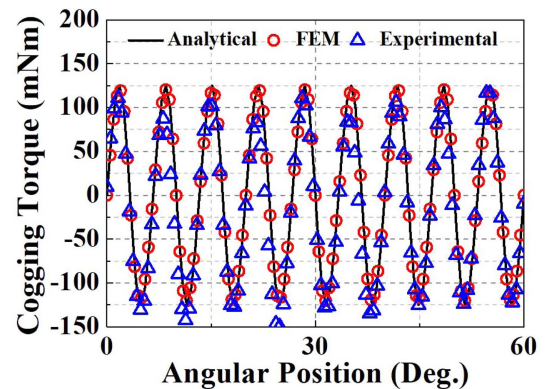

Fig. 9. (Color online) Cogging torque.

measure cogging torque by rotor position through a torque sensor. Figs. 6-8 compare the magnetic flux density results derived through the analytical method and the results derived through the finite element method, and it can be observed that the results conform well. Fig. 9 demonstrates the cogging torque results derived through the analytical method, finite element method, and experiment. It was confirmed that the analysis results were in conformity with the experimental and finite element analysis results, and the validity of the analytical method was verified.

4. Conclusion

In this study, the magnetic field distribution characteristics were determined and cogging torque analysis of a permanent magnet machine was performed using an analytical method. The governing equations and general solutions for each domain were derived, and the magnetic field distribution characteristics were derived through appropriate boundary conditions. In addition, cogging torque was derived using the derived magnetic flux density and Maxwell stress tensor. It was confirmed that the results derived through the analytical method comply well with the finite element method and experimental results. The research results of this paper can be used as a reference for the initial design of permanent magnet machine.

Acknowledgments

References

[1] Z. Q. Zhu, D. Howe, and C. C. Chan, IEEE Trans. Magn. **38** (2002).

[2] T. Lubin, S. Mezani, and A. Rezzou, IEEE Trans. Magn. **46**, 2036257 (2010).

[3] Z. J. Liu and J. T. Li, IEEE Trans. Magn. **43**, 903417 (2007).

[4] Z. J. Liu and J. T. Li, IEEE Trans. Energy Convers. **23**, 926034 (2008).

[5] F. Dubas and C. Espanet, IEEE Trans. Magn. **45**, 2013245 (2009).

[6] T. Lubin, S. Mezani, and A. Rezzoug, Prog. Electromagn. Res. B **25**, 293314 (2010).

[7] L. J. Wu, Z. Q. Zhu, D. Staton, M. Popescu, and D. Hawkins, IEEE Trans. Magn. **47**, 2116031 (2011).

[8] L. J. Wu, Z. Q. Zhu, D. Staton, M. Popescu, and D. Hawkins, IEEE Trans. Magn. **47**, 2104969 (2011).

[9] K. H. Shin, Masters Thesis, Chungnam National University, Korea (2016).

[10] T. Lubin, S. Mezani, and A. Rezzoug, IEEE Trans. Magn. **47**, 2095874 (2011).

[11] Z. Q. Zhu and D. Howe, IEEE Trans. Magn. **29**, 920460 (1993).

[12] Z. J. Liu and J. T. Li, IEEE Trans. Energy Convers. **23**, 926034 (2008).

[13] D. Zarko, D. Ban, and T. A. Lipo, IEEE Trans. Magn. **44**, 908652 (2008).

[14] L. J. Wu, Z. Q. Zhu, D. Staton, M. Popescu, and D. Hawkins, Int. Conf. Electr. Mach. **59**, 2143379 (2010).

[15] H. K. Lee, Masters Thesis, Chungnam National University, Korea (2020).